PROCEEDINGS, 42nd Workshop on Geothermal Reservoir Engineering
Stanford University, Stanford, California, February 13-15, 2017
SGP-TR-212

# Noble Gas Release and Flow Through a Granite and Basalt

Stephen J. Bauer[1], W. Payton Gardner[2], Hyunwoo Lee[3]

Geomechanics Dept., MS 1033, Sandia National Laboratories, Albuquerque, NM, 87185>

sjbauer@sandia.gov[1]; payton.gardner@mso.umt.edu[2]; lhw615@unm.edu[3]

**Keywords:** Noble gas, rock deformation, deformation sensor

## ABSTRACT

An experimental system we developed combines triaxial rock deformation and mass spectrometry to measure noble gas flow before, during, and after rock fracture. Gas flow through a granite and basalt in its unfractured condition allows estimation of "native" permeability. Geogenic noble gas is released during triaxial deformation (real time) and is related to volume strain and acoustic emissions. The noble gas release then represents a signal of deformation during its stages of development. After fracture, gas flow through samples is used to estimate fractured rock permeability.

Noble gases are contained in most crustal rock at inter and intra granular sites. Their release during natural and man-made stress and strain changes represents a signal of deformation in brittle and semi-brittle conditions. The noble gas composition depends on lithology, geologic history, age of the rock, and fluids present. Uranium, thorium and potassium-40 concentrations in the rocks also affect the production of radiogenic noble gases ($^4$He, Ar). Noble gas emission and its relationship to crustal processes have been studied for many years in the geologic community including correlations to tectonic velocities and qualitative estimates of deep permeability from surface measurements, finger prints of nuclear weapon detonation, and as a potential precursory signals to earthquakes attributed to gas release due to pre-seismic stress, dilatancy and/or fracturing of the rock. Helium emission has been shown as a precursor of volcanic activity.

We present empirical results of gas flow through (permeability estimates) and relationships of specimen strain, microstructural evolution, acoustic emissions, and noble gas release from laboratory triaxial experiments performed upon a granite and a young basalt.

## 1. INTRODUCTION

Noble gases present in crustal rocks are derived from groundwater (atmospheric origins), magmatic activity (mantle origins), and radioactive decay of natural radioactive elements (e.g. U, Th, and K). Radiogenic noble gases are produced within minerals and retained to different degrees within the minerals. The composition of gases within the mineral phase is a function of the mineralogical composition, the rock matrix and the thermal, tectonic, erosional and depositional history of the formation. These gases migrate to the adjacent pore fluid and/or fracture networks over geological time periods via diffusion, recoil and chemical dissolution. Transport of gases occurs within the rock grain, along grain boundaries, in the pore fluid and within the micro to macro fracture network. The transport is a function of the stress state of the rock and its control on chemical processes and the physical configuration of the grain and fracture networks. The work we present investigates the release of these gases as a function of the systematic change in stress state by application of stresses sufficient to fracture the rock.

Noble gas emission and its relationship to crustal processes have been studied for many years [Porcelli, et al, (2002); Ballentine and Burnard (2002)]. For example, helium isotope composition in the Basin and Range are highly correlated to tectonic velocities and provides a qualitative estimate of deep permeability from surface measurements [Kennedy and van Soest (2007)]. Anomalies in helium isotope composition from the regional trend are indicative of higher permeability and heat flow at depth and can be used to identify potential geothermal resources [Kennedy and van Soest (2007)].

Noble gas isotopes are commonly used as a finger print of nuclear weapon detonation. Detection of radiogenic noble-gases released during fission provides a signal of sub-surface nuclear weapons detonation. Gas concentrations significantly above background levels at or beneath the surface of a suspect site during an on-site inspection is generally considered to be an extremely strong indicator of the recent occurrence of an underground nuclear explosion [Carrigan and Sun (2012)].

The potential for radiogenic gas release to give a precursory signal to earthquakes has been investigated in several field studies. Increases in radiogenic gas have been observed and attributed to gas release due to pre-seismic stress, dilatancy and/or fracturing of the rock [e.g. Immè and Morelli (2012); Giardini, et al (1976); Mizutani, et al (1977)]. Post seismic anomalies of $^4$He isotopic composition have been observed in spring water [Bräuer, et al (2003)]. Radiogenic noble gases (radon and thoron) have been observed to respond to earthquakes in Taiwan [Yang, et al (2005)].

Gas release resulting from rock deformation/degradation could be used as means to detect borehole deformation. We postulate that different lithologies could exhibit a unique gas release signature, which is a function stress, strain, and or permanent deformation in a given formation. Once the signature is determined, monitoring an annulus for gas release may provide insight to depth and timing of deformation within the borehole.

From the previous field observations of noble gas sensing and our work we imply that detection of gas may be used to sense, and quantify rock fracture at depth, for example in stimulation scenarios, such as that postulated in an engineered geothermal system.

Laboratory studies of gas released from rock fracture have been completed [e.g. Honda, et al, (1982), Mollo, et al, (2011)]. These tests include gas analyses which are performed at infrequent intervals either when deformation was halted mid test [Mollo, et al, (2011)] or post-test after fracture [Honda, et al, (1982)]. Honda, et al, (1982) developed a relationship between deformation and $^{40}Ar$ release, no relationship was evident for $^{4}He$. Tuccimei, et al, (2010) measured real-time Rn emission during rock deformation. They collected Rn release data in step wise load increments in unconfined test samples and developed relationships between Rn release and deformation amount.

In this study we make continuous measurements of noble gas ($^{4}He$ and $^{40}Ar$) release at elevated confining pressure, simulating environmental conditions in the crust. These data provide information on the mechanics and timing of gas release. Because of the small molecular size, $^{4}He$ is extremely hard to contain. By measuring real-time, with a direct inlet to high-sensitivity mass spectrometers we capture most of the $^{4}He$ released during deformation. The combination of high pressure triaxial experimental rock deformation testing with a high vacuum quadrupole mass spectrometer (QMS) is unique, and preceded by Bauer, et al, (2016) who used $^{4}He$ flow to estimate permeability and $^{4}He$ release to signal deformation using a helium leak detector.

The amount of gas liberated is dependent upon the amount present and that made accessible during deformation. Gas is released during deformation due to the creation of new fracture surfaces, comminution of mineral grains, liberation of gas stored along grain boundaries. Relationships between the surface area of the microfracture regions and the volume strain may be developed from data sets like the one we present; these relationships will depend upon various factors such as the aspect ratio and number density of newly created microcracks. Our study provides a unique data set to analyze deformation and gas release with temporal resolution.

## 2. MATERIALS AND METHODS

The basalt studied was collected by the USGS in Hawaii for this study and is from a 50-year old flow by Frank Trusdell. The basalt is fine grained and contains small vesicles and from x-ray diffraction analysis is composed of labradorite, enstatite, and diopside (Figure 1) with a porosity of 15%. This rock was selected for study because we wanted to test a young basalt, hoping it would contain sufficient levels of geogenic noble gas for detection.

The Westerly granite is a fine grained granodiorite; samples were taken from an oriented block of quarried material used by Krech, et al, (1974) to describe this member of the standard rock suite for rapid excavation. The granodiorite has massive, fine-grained and equi-granular texture and has a modal analysis of plagioclase (43.0%), microcline (22.0%), quartz (24.6%), biotite (6.9%), muscovite (2.0%), zircon (1.0%), and magnetite (0.9%) and a porosity of 1-2%. The Westerly granite was selected because it has been used for numerous studies in experimental rock deformation [e.g. Brace, et al (1966); Tapponnier and Brace (1976)] and is known to contain fluid inclusions [Hall, and Bodnar (1989)], which represent potential gas reservoirs in the rock (Figure 1).

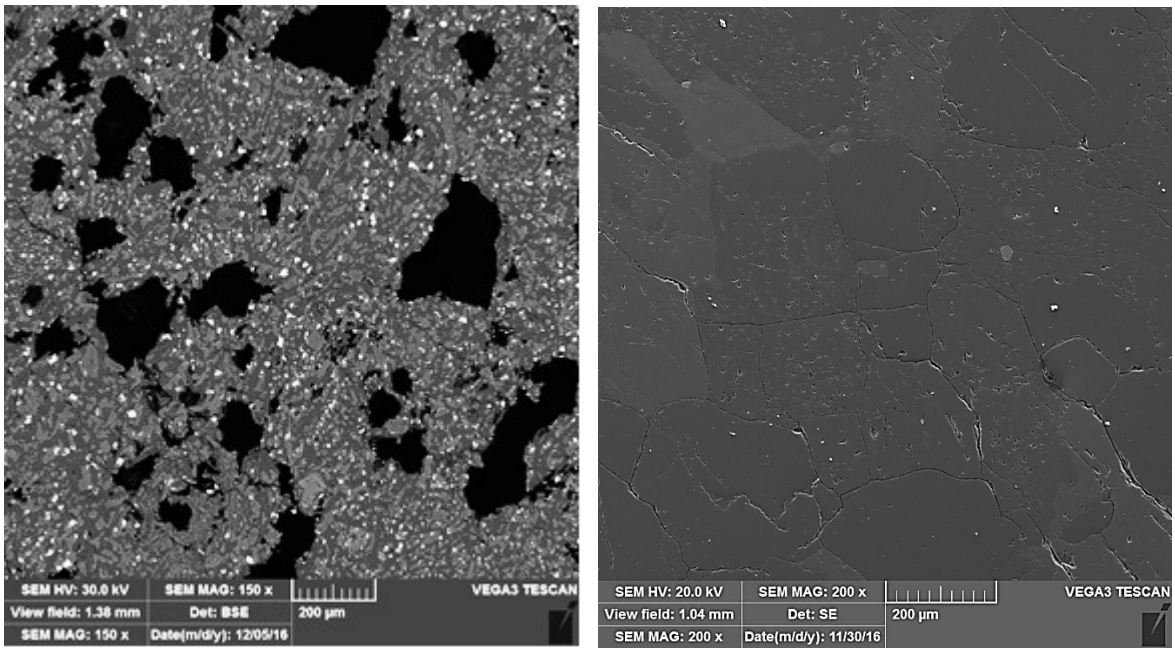


Figure 1. SEM image of basalt (left) and granite demonstrative of the difference in grain size and pore structure

The mechanical portion of the test system consists of a triaxial cell(s) in a variety of loading frames, with the capability of triaxial testing of cylindrical samples ranging from 2.5 cm in diameter (5 cm long) to 10 cm diameter (20-25 cm in length). The greater the sample size the greater the gas release potential because geogenic gas content relates to the amount of material and strain. The triaxial cells are capable of confining pressures to 400 MPa with sufficient axial force (stress) capabilities to fracture rock in compression/extension. The mechanical test system has a pore-fluid flow-through capability used with high pressure (to simulate pore pressure at depth) and low pressure (in the present application of high vacuum). The vacuum pressures achieved required adaptations of vacuum lines of the analytical devices to high pressure lines of the triaxial test system.

The residual gas analysis portion of the test system utilizes mass spectrometry, which measures the mass-to-charge ratio abundance of gas-phase ions [Sparkman (2000)]. In our experiments, the mass spectrometer continually scans for gases during the deformation. We use two different mass spectrometers: a helium leak detector which measures the flow rate of mass 4 and a QMS capable of scanning the total abundance of gas over a broad mass range.

The helium leak detector, an Oerlikon Leibold Phoenix L300i. is a specialized mass spectrometer which we use to detect only $^4$He. It works in the mass range of 2, 3, 4 amu, with a minimum detectable leak rate in vacuum mode of $<5x10^{-12}$ mbar l/s; vacuum runs at about $10^{-3}$ mbar. Time constant of the leak rate signal is <1 s, and the filament is Iridium/Yttria-oxide. For the helium only measurements, a liquid nitrogen trap is in line with the flowing gases to protect the vacuum line.

The QMS is a Pfeiffer HiQuad$^{TM}$ (Figure 2), for analysis of neutral particles with a mass range from 1- 340 amu. The scan speed is 0.125 ms- 60 s/amu; typically, full scan time for a suite of gases (10 species) is on the order of 1-2 seconds. The analyzer is a QMA 410, with a cross beam ion source and a detection limit at 1 x $10^{-15}$ mbar. The detector is SEV 217/Faraday, and the filament is tungsten. The maximum operating pressures are Faraday $10^{-4}$ mbar and SEM $10^{-5}$ mbar. For these measurements, an acetone/$CO_2$ trap is in line with the flowing gases to protect the vacuum line. The software which is used to operate the HiQuad$^{TM}$ is Quadera®, with a LabVIEW® based user interface for data acquisition and control. The vacuum line was by designed by W. P. Gardner. The analytical devices are semi-portable, located on a rolling cart so that all triaxial frames in the lab are accessible.

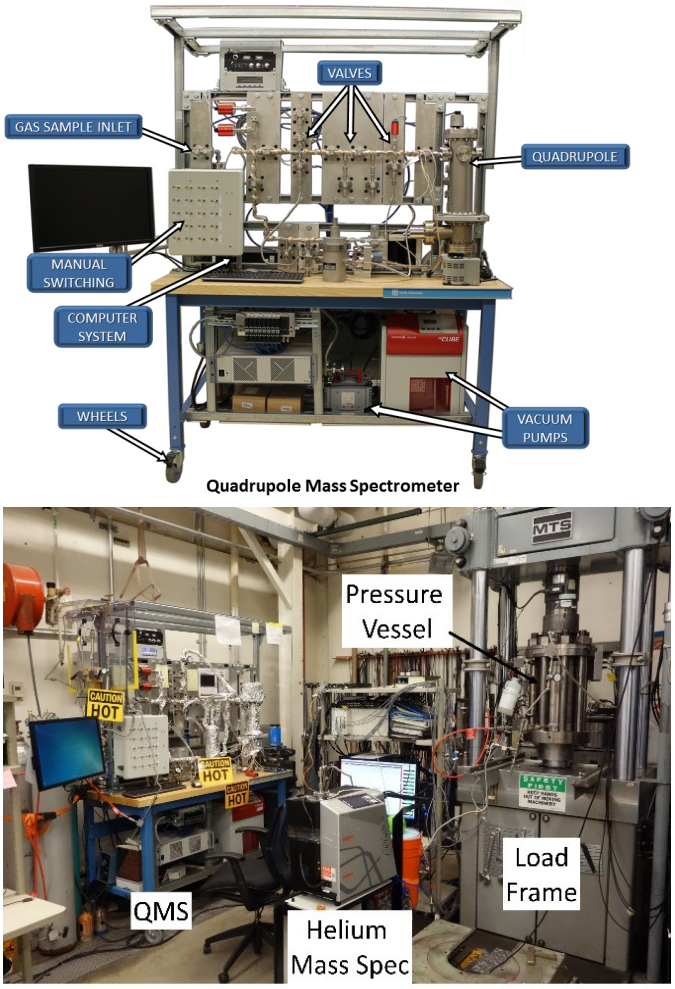


Figure 2. Quadrupole Mass Spectrometer (QMS); Test system

Two experiments are reported upon: one using the helium leak detector for the granite, and the second using the QMS for the basalt. The helium leak detector recorded the $^4$He release rate during the deformation as a volume flow rate and is displayed in this paper as volume release versus time. The QMS was used to observe changes in gas composition, and the $^4$He and $^{40}$Ar mixing fractions in parts per million (ppm) are presented as a function of time.

The helium leak detector is also used for the permeability measurements using a test method described in Lee and Bauer (2015) because of the tightness of these rocks before and after deformation. Separate samples are used for intact/unfractured material testing (so as not to contaminate samples with helium), and the test samples themselves are used in the fractured state to estimate the fractured rock permeability. Darcy's law is expressed as the measured flow rate of fluid crossing a unit area and is proportional to the pressure differential measured across the ends of the specimen. The permeability of the rock, k, is estimated by the following equation:

$$k_{app.} = Q_x \cdot \mu \cdot L / (A \cdot \Delta P) \quad (1)$$

where $k_{app.}$ is the apparent permeability (Darcy), $Q_x$ is the flow rate recorded through the mass spec in the axial direction ($cm^3/s$), $\mu$ is the viscosity of flowing helium (cP), $\Delta P$ is the pressure differential measured across the ends of the specimen (atm), our upstream pressure is 1-2 atm, L is the length of the specimen (cm), and, A is the cross-sectional area ($cm^2$) perpendicular to the axis of the specimen. Here, Darcy's law in equation (1) assumes an incompressible medium. For the compressible helium gas, the volumetric flow rate Q varies with pressure from one face of the specimen to the other. Assuming that the pressure of the outlet (or "discharge") side is close to zero due to vacuum condition, equation (1) can be modified for a compressible fluid such as helium:

$$k_{He} = 2\, Q_{in} \cdot \mu \cdot L / (A \cdot \Delta P) \quad (2)$$

where $k_{He}$ is the permeability measured using helium and $Q_{in}$ is the volumetric flow rate in the inlet side of the specimen. Thus, using the equation of state of the gas under constant temperature, $k_{He}$ is related to the apparent permeability ($k_{app.}$) based on incompressible fluid as follows:

$$k_{He} = 2\, k_{app.}\, Q_{in} / Q_{ref} = 2\, k_{app.}\, P_{ref} / P_{in} \quad (3)$$

where $P_{ref}$ is the reference pressure when $Q_{ref}$ is measured and $P_{in}$ is the pressure on the inlet side. Klinkenburg corrections are not presented in the results shown.

### 2.1 Experimental Setup

For the triaxial deformation setup, samples are assembled as shown in Figure 3. The rock sample is ground for parallel and perpendicular conditions as per ASTM standards. The samples are right circular cylinders, nominally 3.8 cm in diameter and 8 cm in length and oven dried for a week at 50°C prior to testing. Lateral displacements are measured with displacement transducers or strain is directly recorded with strain gages. Figure 3 shows the transducer setup in which buttons are glued directly to the sample along a diameter near the sample midheight. Axial displacement transducers are affixed to the sample end caps. Four acoustic emission transducers are attached to the sample at quarter perimeters; acoustic emissions are counted if similar signals are triggered in at least three of the four transducers within a specified time window. The sample is sandwiched top and bottom between an alternating layer of pressed metal fiber mesh and steel spacers to assure gas flow accessibility; the sample is then jacketed first with a thin layer of UV cure urethane. This layer adheres tightly to the rock surface inhibiting gas flow along the rock surface. A sleeve of polyolefin shrink tube is placed over the first layer of UV cure urethane, and is then encapsulated in another layer of UV cure urethane. This jacketing procedure has proved successful in avoiding jacket leaks during rock fracture events.

Test specimens are instrumented to measure axial and radial displacements during application of the initial hydrostatic pressure, and during axial compression portion of the test (Figure 3). Displacement is measured with four Linear Variable Differential Transformers (LVDTs): two LVDTs mounted on the end caps to measure axial deformation, and two mounted in spring loaded rings placed near the sample midheight to measure change in diameter. LVDT displacements are averaged to calculate strain; the actuator has a separate LVDT that can be used as a backup to on-sample axial measurements. Sample mounted LVDTs are 0.254 cm full-scale. Displacement is used to calculate sample strain and stress is calculated using the measured force and updated cross sectional area based on lateral displacements.

Jacketed and instrumented specimens were placed onto the base of the pressure vessel and connected to pore-pressure feed-throughs in the pressure vessel. The pressure vessel was then assembled and placed into the reaction frame. The actuator in the base of the frame is raised gradually to bring the pressure vessel piston into contact with the reaction frame. The pressure vessel is then connected to the pressure intensifier and filled with Isopar®. After the specimen/pressure vessel system was assembled and placed into the load frame the pressure vessel is filled with confining fluid (Isopar H®). The sample is subjected to 1-2 MPa confining pressure and then the vacuum system is applied to the pore pressure access to the sample. The sample is first degassed at low pressure, and then test confining pressure is applied and held at approximately test pressure while the specimen continued to degas for another 24 hours.

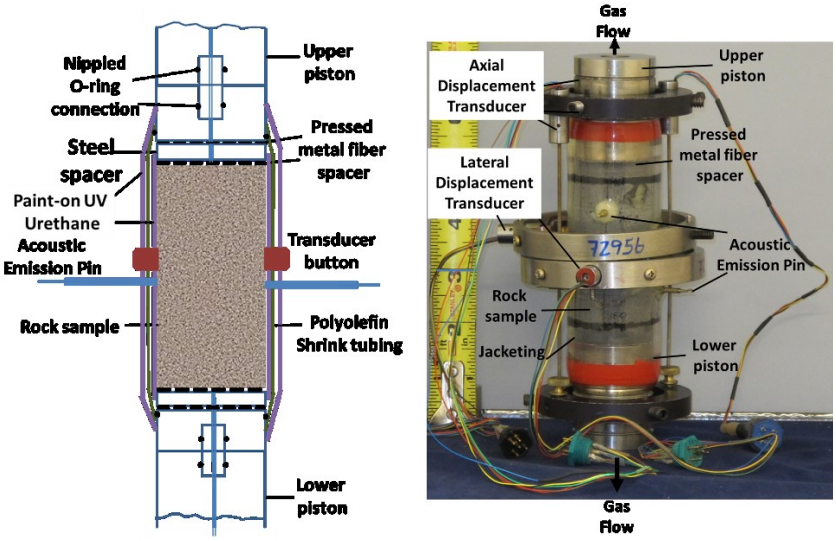


Figure 3. Typical sample assembly: A: schematic; B: actual.

During the experiment, confining pressure is controlled, measured and tracked using a pressure transducer located in the intensifier connection line about a meter from the pressure vessel. Axial force is measured with a load cell external to the pressure vessel and O-ring friction is corrected during data analysis. The specimen was deformed using a controlled displacement mode and shortened at a rate of approximately $5x10^{-6}$ $s^{-1}$. Force, displacement, acoustic emissions, confining pressure and gas flow were recorded in an automatic data acquisition/control system as a function of time.

## 3 EXPERIMENTAL RESULTS

### 3. 1 Permeability Estimates

Permeability measured on unfractured and fractured granite and basalt is given in Table 1. The permeability of granite is slightly greater than that of basalt, this relates to the initial porosity and pore structure. Fracturing of both rocks promotes a greater increase in permeability of granite than the basalt.

Table 1. Permeability estimates

| Lithology | Condition | Porosity (%) | Confining pressure (MPa) | Estimated Permeability (μD) |
|---|---|---|---|---|
| Westerly granite | unfractured | 1-2 | 13.8 | .19 |
| Westerly granite | fractured | | 13.8 | 12.70 |
| Hawaiian basalt | unfractured | 15 | 27.6 | .14 |
| Hawaiian basalt | fractured | | 27.6 | .18 |

### 3. 2 Triaxial and Gas Release Measurements

Here we report triaxial deformation data from two experiments, WG4 and HB3; the granite sample is deformed at 13.8 MPa confining pressure and the basalt is deformed at 27.6 MPa confining pressure and both used axial strain rates on the order of $10^{-6}$.

For the Hawaiian basalt, we unfortunately lost lateral deformation gages in this test, thus quantification of volumetric deformation is unavailable and results are presented in relation to the axial deformation. The sample yielded and has an ultimate strength near 240 MPa, and then work softened before it was unloaded (Figure 4).

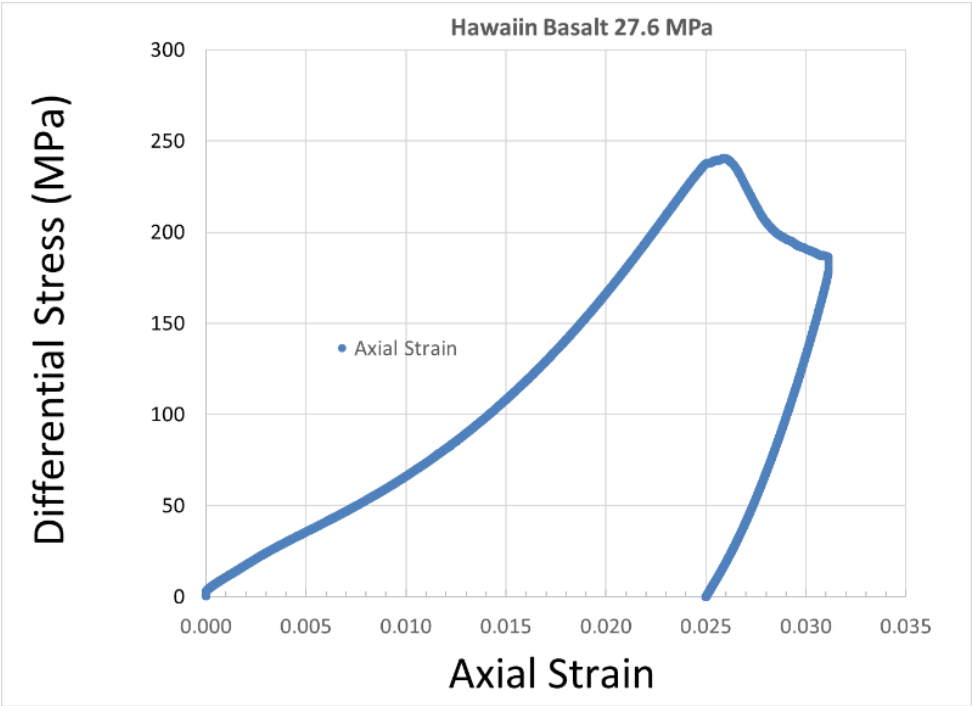


Figure 4. Differential stress versus axial strain for Hawaiian basalt.

Real time release of helium and argon, cumulative acoustic emissions and axial strain versus time are shown in Figure 5. Important observations from this plot include the initiation of noble gas release at 1/3 to 1/2 of the maximum axial strain, gas release "peaking" near and at yield of the sample, near background release when unloading of the sample begins, coupled with acoustic emission initiation at about the same timing as gas release (perhaps a bit later). No gases are released nor acoustic emissions sensed during hydrostatic pressurization, indicating pores did not collapse. The noble gas release is episodic during axial loading.

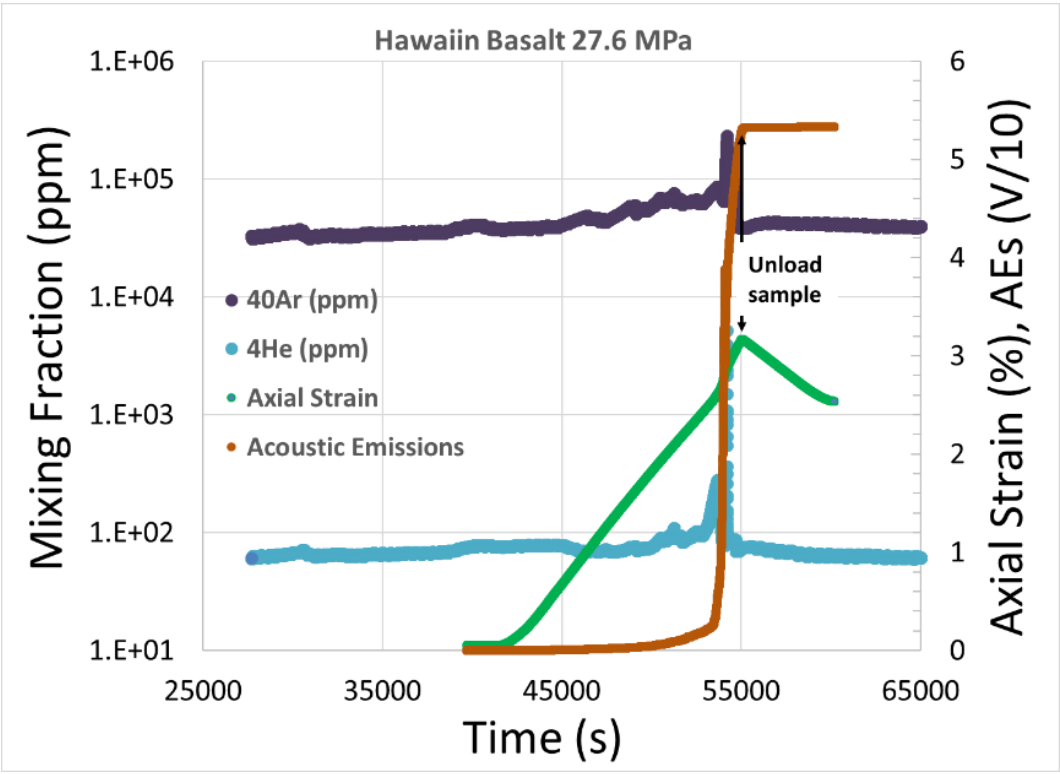


Figure 5. Argon and helium mixing fraction, axial strain and cumulative acoustic emissions versus time for Hawaiian basalt

For the Westerly granite lateral, axial and volume strain components were determined (Figure 6) allowing direct comparisons of helium gas release and acoustic emissions versus time. Helium release, here sensed as a continuous monitoring of flow rate (Figure 7), begins to

increase at 1/3 to 1/2 of the maximum axial strain. The flow rate peaks at or near the maximum axial strain, and then drops off to background levels. In this test, acoustic emissions begin to increase at ~ 1/2 of the maximum axial strain, and accumulate much faster once dilatant behavior is prevalent Figure 8.

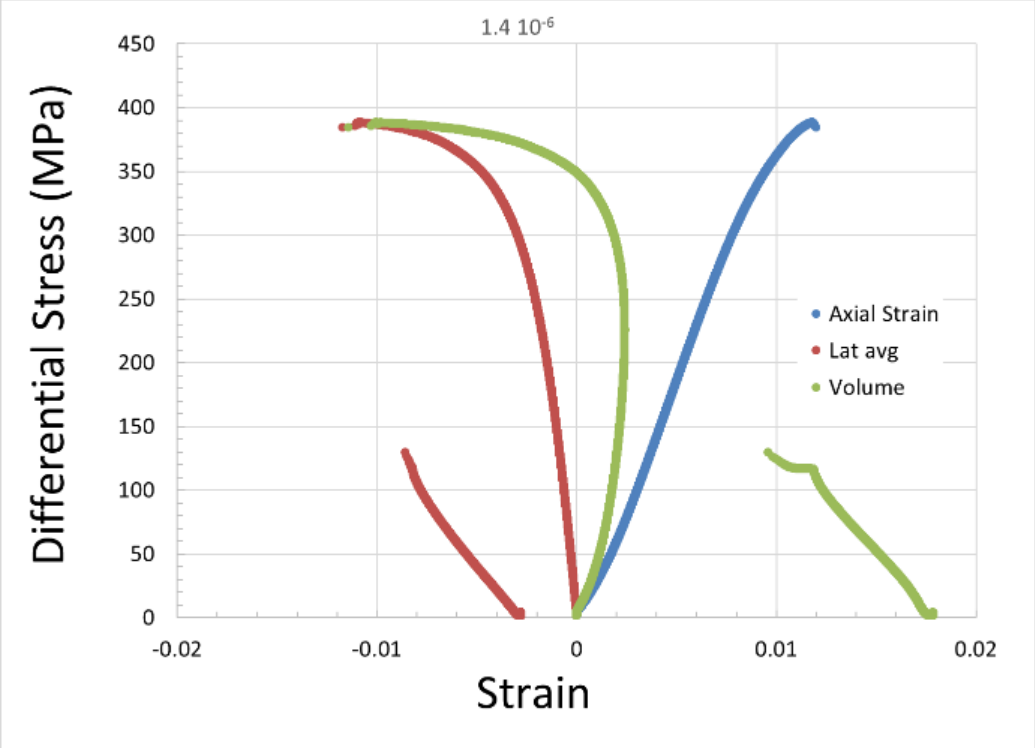


Figure 6. Differential stress versus strain components for Westerly granite.

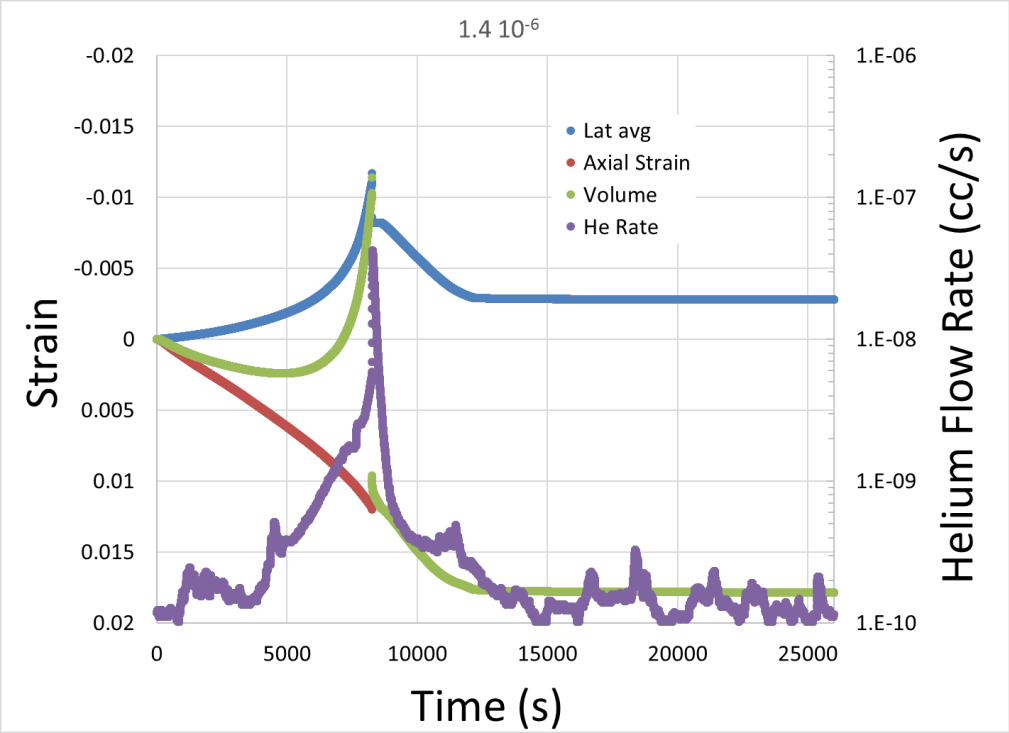


Figure 7. Strain components and helium flow rate versus time for Westerly granite.

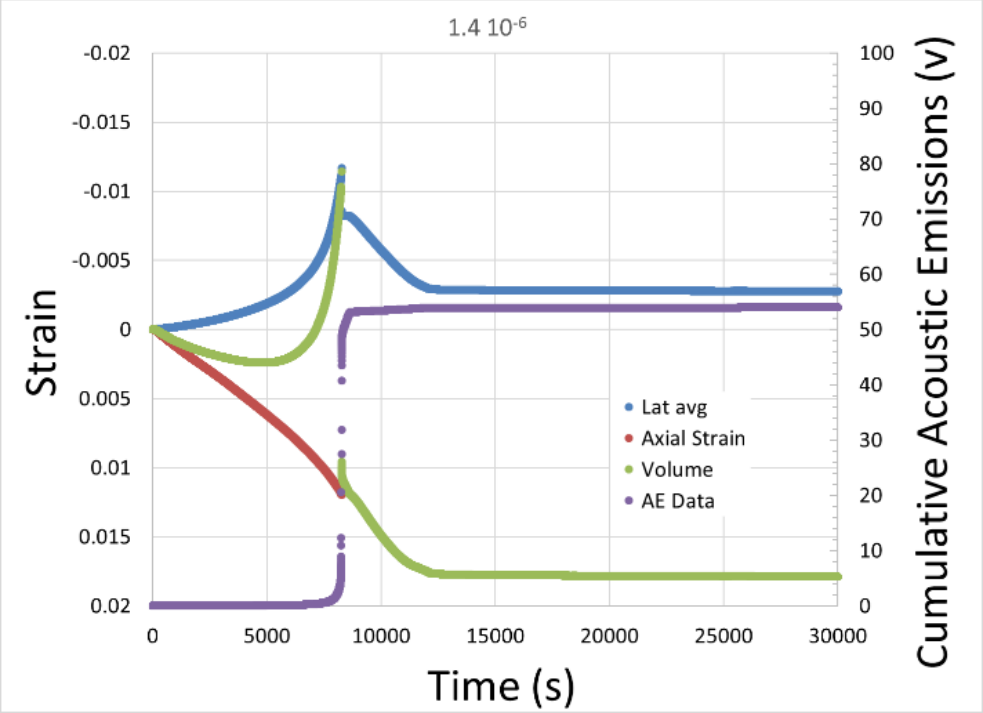


Figure 8. Strain components and cumulative acoustic emissions versus time for Westerly granite.

The helium flow rate versus time data allows us to calculate the amount of helium released during the test (simply it is the area under the curve in Figure 7) and is plotted versus volume strain in Figure 9. Also plotted are compaction and dilatant conditions of the test. We observe that gas is released during the compaction phase of the deformation, indicating that some new cracks are being formed during compaction, --here manifested as gas release. As more cracks form, the flow rate increases, as does the total amount of gas released. Gas release ceases shortly after s fracture of the sample.

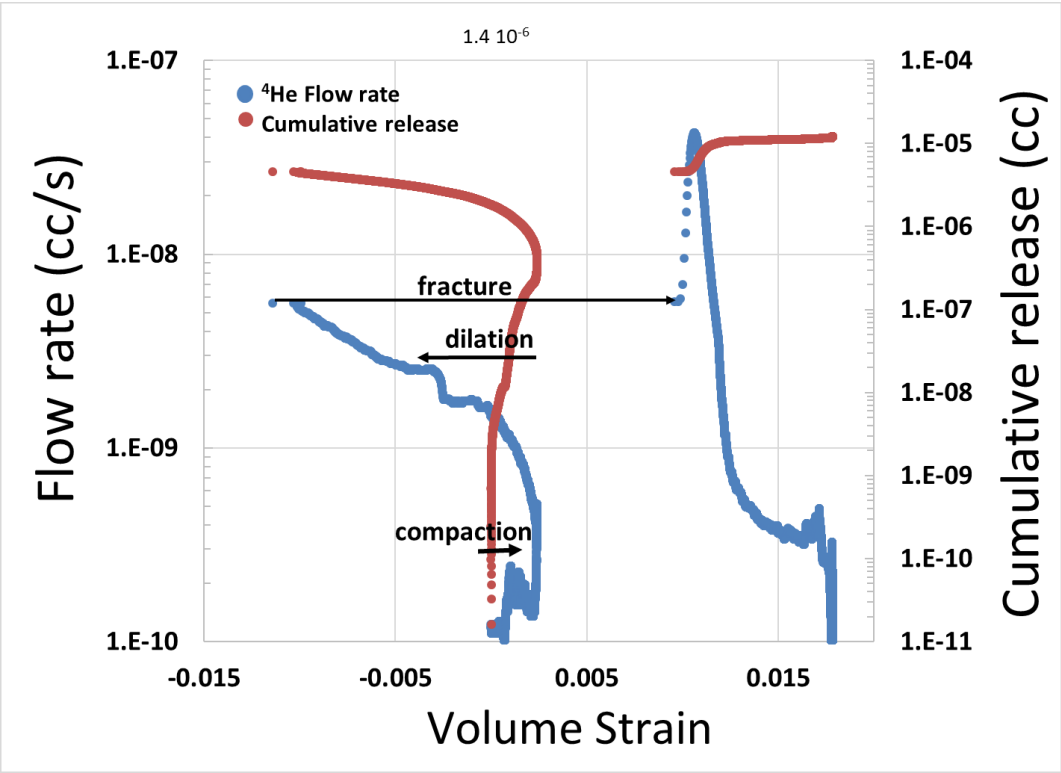


Figure 9. Helium flow rate and cumulative helium released versus volume strain for Westerly granite.

### 3.1 Observations

Each sample was studied post mortem using optical and scanning electron microscopy. The basalt was observed to deform by first collapse of some vesicles, pervasive development of intragranular microfractures and development of a throughgoing fracture (Figure 10, 11). The basalt contains intergranular vesicles and intragranular micropores; they both represent likely residence sites of noble gases; noble gases may be contained in the mineral lattice as well.

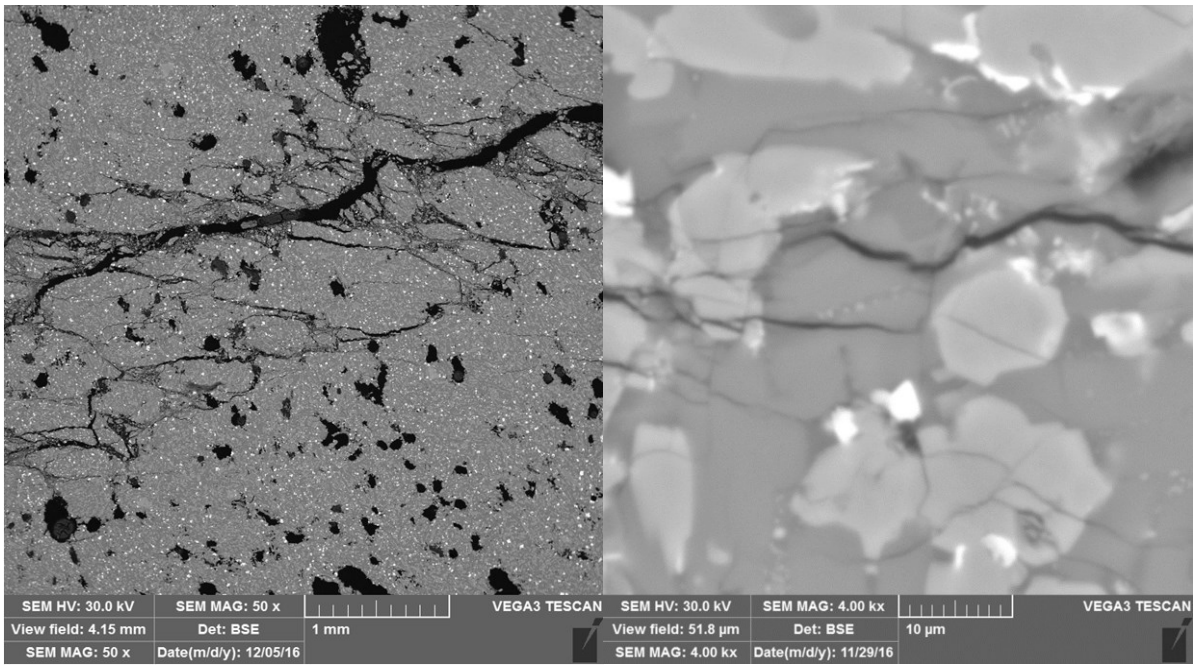


Figure 10. Central shear zone in deformed basalt (left). Note flattening vesicles, axial fractures coalescing to form the shear zone and locally intense regions of deformation; loading is horizontal. (Right) intense local microfracturing.

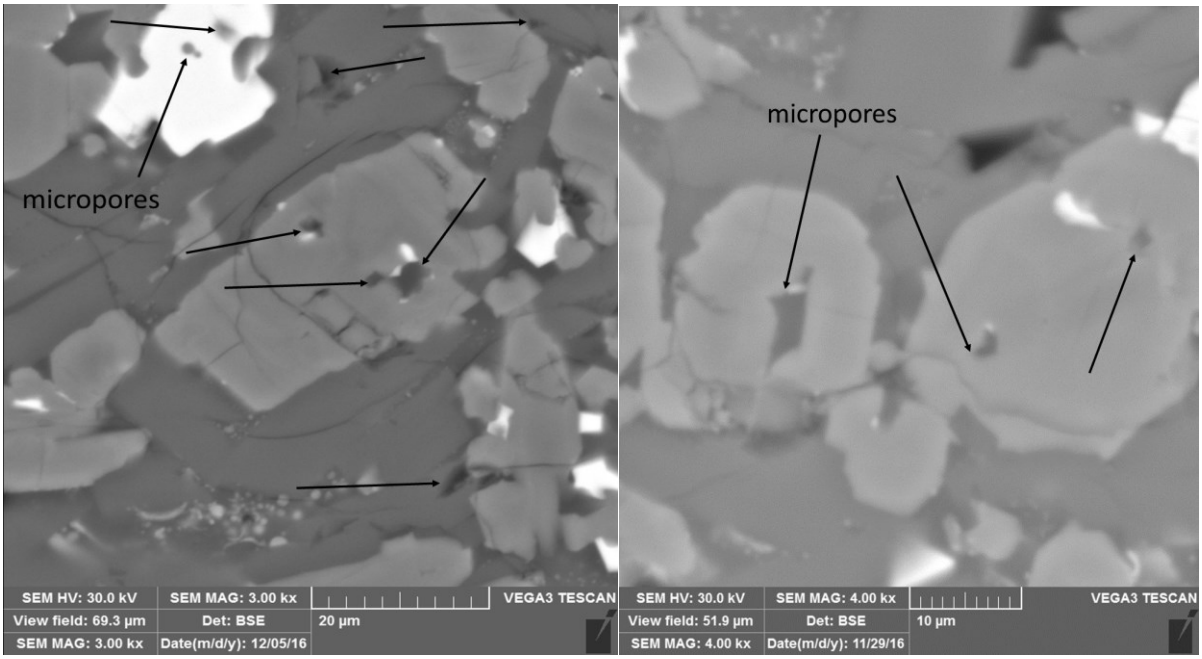


Figure 11. Micropores in basalt, potential sites of gas release.

The Westerly granite was observed to deform by pervasive systematic development of inter and intragranular microfractures as the differential stress is increased, and development of a throughgoing fracture. Intersection of microfracturing with intracrystalline micropores (Figure 12,13), and lattice trapped gases led to continuous release of noble gases (here helium).

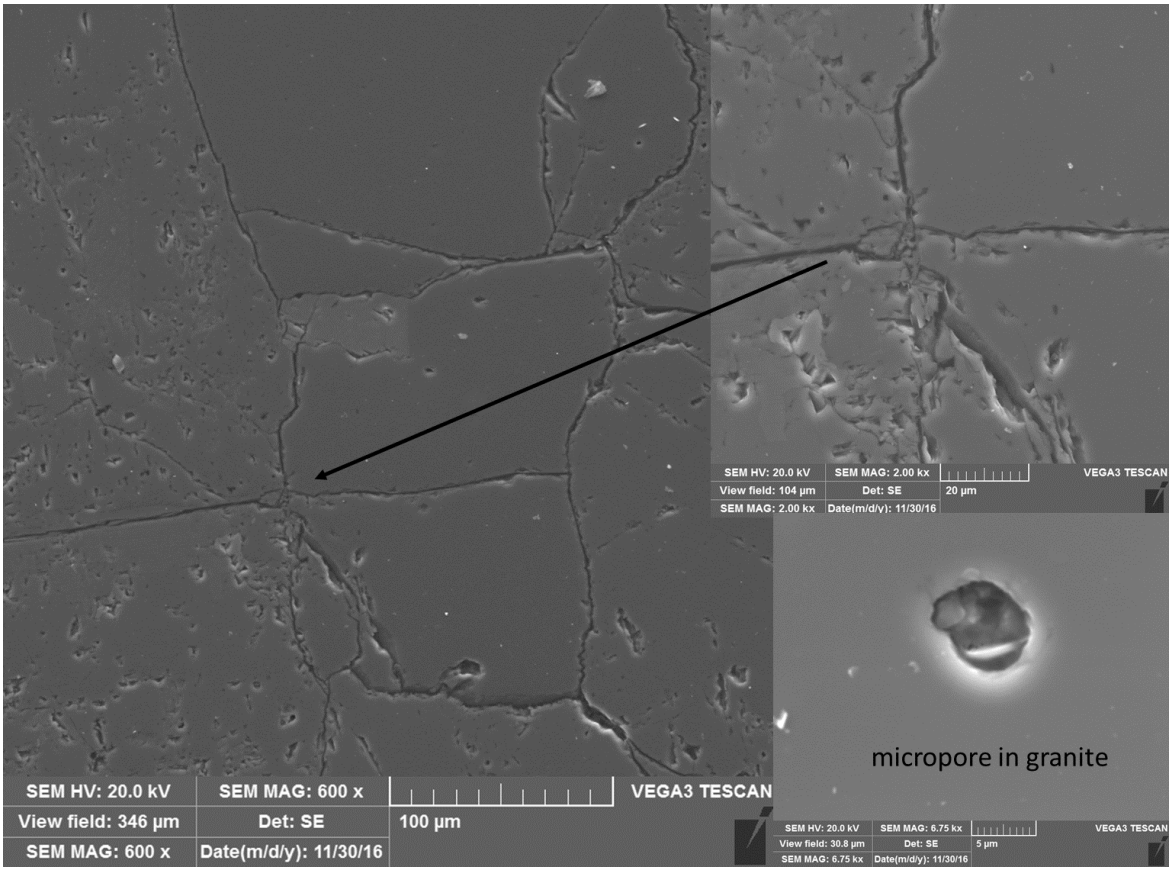


Figure 12. Stress induced microcracks in Westerly granite; inset: micropore represents a potential site from which noble gases are released.

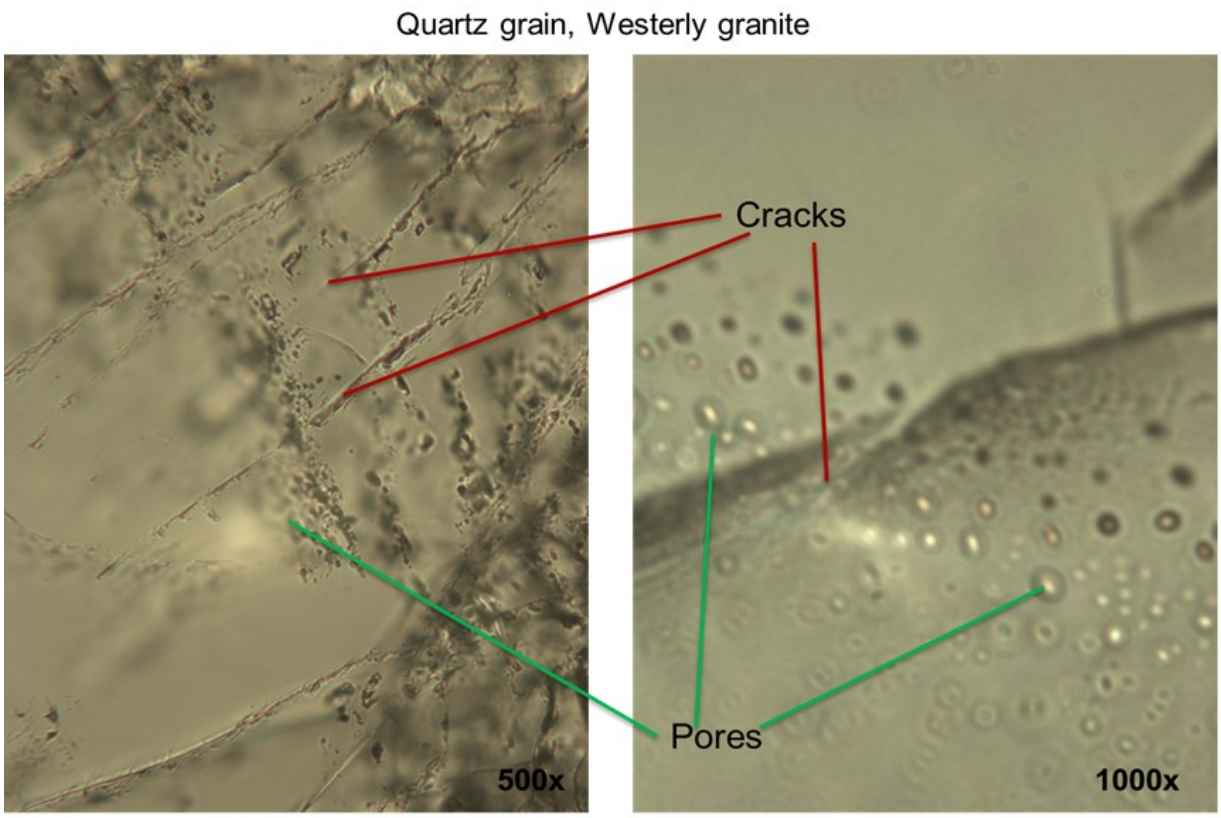

Figure 13. Microcracks intersecting micropores in Westerly granite.

## 4. DISCUSSION OF RESULTS AND CONCLUSIONS

The following results are suggested from the work presented; (1) noble gases are released and measured real time during deformation; (2) the noble gas release signal is precursive to macrofracture; (3) gas released depends on initial gas content, pore structure and its evolution during deformation, deformation amount, and permeability; (4) release rate increases as strain and microfracturing increase; (5) Gases are released from intracrystalline sites.

The release of noble gases for both granite and basalt, quantified using two analytical tools shows an apparent cause and effect relationship between the accumulation of strain and noble gas release. The initial pore structure in each the granite and basalt are different to start; the dominantly aphanitic and vesicular basalt compared to the phaneritic medium to fine grained granite.

For the granite, early in the test, noble gas release rate increase slightly as the sample is initially loaded and compacted in the axial direction. During this time noble gas release pathways are being closed, yet gas is released because it is being generated by microcrack formation; the helium is quite mobile, and escapes to the detector. As stress and strain progresses, cracks subparallel to the flow direction are created and appropriately oriented pre-existing cracks open through well understood processes. These new cracks provide access to release stored radiogenic noble gas, and the new and existing cracks provide noble gas transport pathways, thus more helium is sensed. This crack/access/flow process continues as the deformation progresses, becomes more pervasive, and is eventually manifested in the macrofracture, all the while, helium flow rate (gas release) increases. The macrofracture enhances release potential because it connects many microfractures and it represents a connected flow conduit. Mineral grains in the fracture vicinity can also be ruptured, releasing more noble gas through diffusive process. Once the throughgoing fracture forms, the test is stopped, and the release of helium diminishes. The reservoirs of helium which were opened by fracturing have been drained; new fracturing would be needed to release more helium.

As the basalt deforms, vesicular collapse begins early in the deformation, and is coupled with microfracturing, and culminates in a macrofracture. It is possible that early releases of gas in basalt correlate to vesicle fracture. Intragranular fractures are sensibly small, and many are required to fully develop a fracture network.

Each of these analytical methods represents means to evaluate rock deformation. By measuring real-time release of the gases during deformation, we are allowed to directly connect gas release to crack creation and extension.

$^{4}$He and $^{40}$Ar release observed in these tests is sensitive to the structural evolution of the sample during deformation and can be used to infer some of the major processes occurring throughout deformation. These experiments indicate that the noble gas release signal is sensitive to the details of the mechanical deformation, for example crack initiation and propagation and coalescence.

This work provides additional laboratory data sets to support potential field monitoring of the release of naturally occurring $^{4}$He, $^{40}$Ar and other noble gases in the subsurface to monitor changes in stress, strain and permeability in the subsurface for applications including earthquake prediction, volcanic activity, stimulation technologies, borehole integrity, detonation detection, and nuclear waste disposal.

These experiments, coupled with detailed observation of operative process at each step of the deformation, using for example acoustic emissions, will provide insight into the relationship between gas release and deformation of the rock. Quantitative interpretation of experiments of this kind could provide the basis for developing constitutive relationships between mechanical deformation, gas release and permeability, and the ability to use naturally occurring as well as doped tracers to observe and monitor mechanical deformation.

## 5 ACKNOWLEDGEMENTS

The authors thank Perry Barrow and Mike Hileman for their contributions to portions of the experimental work. Frank Trusdell of the USGS collected the basalt samples. Melissa Mills took the SEM photomicrographs. This work was partially supported by the Laboratory Directed Research and Development Program at Sandia. Sandia National Laboratories is a multi-mission laboratory managed and operated by Sandia Corporation, a wholly owned subsidiary of Lockheed Martin Corporation, for the U.S. Department of Energy's National Nuclear Security Administration under contract DE-AC04-94AL85000. SAND2017-1271 C.

## 6 REFERENCES

Porcelli, D., Ballentine, C. J. and Wieler, R.:(Eds.) (2002) Noble Gases in Geochemistry and Cosmochemistry. Mineralogical Society of America 47.

Ballentine, C. and Burnard, P.: (2002) Production, Release and Transport of Noble Gases in the Continental Crust. Mineralogical Society of America 47.

Kennedy, B., and van Soest, M. C.:(2007) Flow of Mantle Fluids through the Ductile Lower Crust: Helium Isotope Trends. Science 318, 30.

Carrigan, C. R., and Sun, Y.: (2012) Detection of Noble Gas Radionuclides from an Underground Nuclear Explosion During a CTBT On-Site Inspection. Pure Appl. Geophys., Springer Basel AG, DOI 10.1007/s00024-012-0563-8.

Immè, G., and Morelli, D.: (2012) Radon as Earthquake Precursor in Earthquake Research and Analysis - Statistical Studies, Observations and Planning, S. D'Amico, In Tech pub. 460pp.

Giardini, A. A., Subbarayudu, G. V., and Melton, C. E.: (1976) The emission of occluded gas from rocks as a function of stress: its possible use as a tool for predicting earthquakes. Geophys. Res. Lett. 3, 355-358.

Mizutani, H., Spetzler, H., Getting, I. Martin III, R. J. and Soga, N.: (1977) The effect of outgassing upon the closure of cracks and the strength of lunar analogues. Proc. 8th Lunar Sci. Conf. 0977, 1235-1248.

Bräuer, K., Kämpf, H., Strauch, G. and Weise, S. M.: (2003) Isotopic evidence (3He/4He, $^{13}$C-CO2of fluid-triggered intraplate seismicity. J. Geophys. Res.: Solid Earth 108, no. B2.

Yang, T.F., Wali, V., Chyi, L. L., Fu, C. C., Chen, C. H., Liu, T. K., Song, S. R., and Lee, C. Y.: (2005) Variations of soil radon and thoron concentrations in a fault zone and prospective earthquakes in SW Taiwan. Radiation Measurements 40.2: 496-502.

Honda, M., Kurita, K., Hamano, Y. and Ozima, M.: (1982) Experimental studies of He and Ar degassing during rock fracturing. Earth Planet. Sci. Lett. 59; 429-436 429.

Mollo, S., Tuccimei, P., Heap, M. J., Vinciguerra, S., Soligo, M., Castelluccio, M., Scarlato, P., and Dingwell, D. B.: (2011) Increase in radon emission due to rock failure: An experimental study. Geophys. Res. Lett., 38, L14304.

Tuccimei, P., Mollo, S., Vinciguerra, S. Castelluccio, M., and Soligo, M.: (2010), Radon and thoron emission from lithophysae-rich tuff under increasing deformation: An experimental study. Geophys. Res. Lett. 37.

Bauer, S. J., Gardner, W. P., and Lee, H.: (2016) Release of Radiogenic Noble Gases as a New Signal of Rock Deformation., Geophysical Research Letters, 2016GL070876

Krech, W. W., Henderson, F. A. and Hjelmstad, K. E.: (1974) A Standard Rock Suite for Rapid Excavation Research. U.S. Bureau of Mines, RI-7865.

Brace, W. F., Paulding, B. and Scholz, C.H.: (1966) Dilatancy in the fracture of crystalline rocks. J. Geophys. Res. 71, 3939-3954.

Tapponnier, P. and Brace, W. F.: (1976) Development of Stress-Induced Microcracks in Westerly granite. Int. J. Rock Mech. Min. Sci. & Geomech. Abstr. Vol. 13, pp. 103-112.

Hall, D.L., and Bodnar, R.J.:(1989) Comparison of fluid inclusion decrepitation and acoustic emission profiles of Westerly granite and Sioux quartzite. Tectonophysics, 168, p 283-296.

Sparkman, O.D.: (2000) Mass spectrometry desk reference. Pittsburgh: Global View Pub. ISBN 0-9660813-2-3.

Lee M.Y. and Bauer, S.J.: (2015) Development of Helium-Mass-Spectrometry-Permeameter for the Measurement of Permeability of Near-Impermeable Rock. Rock Mechanics and Rock Engineering, DOI: 10.1007/s00603-016-1058-1